Journal of Materials Science: Materials in Electronics (2020) 31:11784–11790
https://doi.org/10.1007/s10854-020-03730-y

Aging characteristic of Cu-doped nickel manganite NTC ceramics

Mo Zhao[1] · Wei Chen[1] · Wei Wu[1] · Maolin Zhang[2] · Zhimin Li[2]

Received: 18 February 2020 / Accepted: 3 June 2020 / Published online: 12 June 2020

Abstract
The drift in electrical properties (e. g., the resistivity and *B*-value) is vital to the practical application for negative temperature coefficient (NTC) ceramics. In this work, Cu-doped nickel manganite ceramics were prepared by solid-state method, to investigate the degradation mechanism of both the resistivity and B-value. Results showed that the as-prepared ceramics exhibited typical NTC characteristics with cubic spinel phase, and that Cu doping greatly reduced the resistivity and *B*-value. However, the increase of Cu content in system aggravated the drift in the resistivity and B-value after the samples were aged at 300 °C for 30 h. XPS was carried out to further clarify the change in electrical properties. It was found that the decline of properties was due to the decrease of Mn^{4+} content in system after aging, which derived from the increase of chemical valence of Cu.

1 Introduction

Negative temperature coefficient (NTC) ceramic thermistors are the temperature sensing devices characterized by decreased resistance as working temperature increases [1–3]. Because of high sensitivity and low cost, they have been widely used in temperature measurement and compensation, overheat protection, surge current suppression, etc. [4–7]. Among NTC materials, transition metal manganites with spinel structure have recently been paid much attention for their superior properties [8]. The two important parameters, i.e., room temperature resistivity and $B_{25/85}$ value, are always employed to evaluate the external response of these materials [9–11]. For oxides with spinel structure, their electrical properties are strongly related to the imperfection (e. g., impurity defects) in crystal. Accordingly, cation doping has been considered as an effective method to tailor the room temperature resistivity and $B_{25/85}$ value for transition metal manganites, to further meet various requirements [12], including Zn [13–15], Cr [16], Al [17], Mg [18], Ti [19], Fe [20], Ba [21], and B [22] ions.

In practical application, the drifts in resistivity and $B_{25/85}$ value due to aging or long-time use are also crucial for NTC materials. Until now, several strategies have been used to investigate the drift in electrical properties during aging process, such as the redistribution of cations, the disproportionation between trivalent and tetravalent Mn cations, the change in oxidation state of Mn cations, the reaggregation of cations and electronics, and the reconfiguration of electrode/ceramic interface [23]. As a result, the drift in electrical properties is substantially reduced by doping with impurity elements, selecting suitable electrode materials, and adjusting physical and chemical properties of starting materials [24, 25]. Here, note that large porosity and non-dense bulk also contribute to inferior electrical stability and reproducibility of ceramics [26, 27]. In addition, Yang et al. [6] deposited $Ni_{0.6}Mg_{0.3}Mn_{1.5-x}Al_{0.6+x}O_4$ ($x = 0$–0.6) NTC thick films by developed supersonic atmospheric plasma spray, and identified that it was the impurity phase of $MgAl_2O_4$ that affected NTC properties. Moos et al. [28] reported that suitable heat treatment was helpful to improve aging stability of NTC materials.

Cu level could directly affect the electrical properties of nickel manganite-based NTC ceramics [11, 29], as well as crystal phases, microstructures and bulk densities. Puri et al. [11] found that the lattice parameters and grain sizes of $Ni_{1-x}Cu_xMn_2O_4$ ($0 \le x \le 1$) ceramics decreased as the Cu content increased, which led to reduced resistance from 44 to 33 MΩ at 30 °C. On the other hand, although the

✉ Mo Zhao
zhaomo@nint.ac.cn

✉ Zhimin Li
lizhmin@163.com

[1] State Key Laboratory of Intense Pulsed Radiation Simulation and Effect (Northwest Institute of Nuclear Technology), Xi'an 710024, China

[2] School of Advanced Materials and Nanotechnology, Xidian University, Xi'an 710071, China

transmission process of Cu^{+} to Cu^{2+} greatly affected the transition probability of localized carriers, resulting in resistance change [7, 20, 30, 31], little direct evidence has so far been provided on the chemical state of Cu and the ratio of Cu^{+} to Cu^{2+}. Furthermore, the introduction of Cu often causes a remarkable resistance drift [32], which makes the degradation mechanism to become more complicated.

In this study, nickel manganite NTC ceramics ($Ni_{0.7}Mn_{2.3-x}Cu_xO_2$, $x=0.1$–0.4) were prepared in an effort to elucidate the roles of Mn and Cu ions in DC resistance, resistance drift, and B-value. XPS was carried out to further distinguish the chemical states of Mn and Cu ions in system. And the corresponding mechanism was discussed in detail.

2 Experimental

2.1 Ceramic preparation

$Ni_{0.7}Mn_{2.3-x}Cu_xO_2$ ($x=0.1$, 0.2, 0.3, and 0.4) NTC ceramics were prepared by solid-state method. Analytically, pure manganese carbonate ($MnCO_3$), nickel trioxide (Ni_2O_3), and copper oxide (CuO) were used as starting materials. The synthesis was carried out by first stoichiometrically weighing these materials. Then, the materials were mixed with alcohol by planetary ball mill for 12 h. Next, the as-obtained slurries were dried at 80 °C for 20 h. And the dried mixtures were fired at 800 °C for 6 h to prepare precursor powders. After mixed with PVA (4 wt%), the powders were pressed to disks with the diameter of 10 mm, which were sintered at 1150 °C for 4 h in air atmosphere. Finally, to measure electrical properties, silver paste was coated on both sides of ceramic samples, and then annealed at 500 °C for 0.5 h. In this study, $Ni_{0.7}Mn_{2.3-x}Cu_xO_2$ samples with different Cu contents (0.1, 0.2, 0.3 and 0.4) were marked as NMC-1, NMC-2, NMC-3, and NMC-4, respectively.

2.2 Aging process

As reported by Metz [25], the optimum aging temperature was 300 °C, and there was a significant increase in the resistivity during initial 24 h. Then, the drift rate tended to decrease drastically. Therefore, the as-prepared NTC samples were heat-treated at 300 °C with a holding time of 30 h in air atmosphere to investigate aging characteristic in this work.

3 Results and discussion

The dependence of resistance on temperature for the as-prepared $Ni_{0.7}Mn_{2.3-x}Cu_xO_2$ ($x=0.1$, 0.2, 0.3, and 0.4) ceramics were measured by resistance–temperature testing system (ZWX-B, Huazhong University of Science and Technology, China). Figure 1 shows the relationship between resistance (R) and testing temperature, and the change in logR as a function of the reciprocal of temperature ($1/T$). As can be seen, the resistance obviously decreases as operating temperature increases from 25 to 130 °C, reflecting typically NTC characteristic [6, 7]. In general, the Arrhenius formula could be used to express the resistivity-temperature relationship of NTC ceramics [33, 34].

$$\rho_T = A\exp\frac{E_a}{kT} = A\exp\frac{B}{T} \tag{1}$$

$$\ln\rho_T = \ln A + \frac{E_a}{kT} = \ln A + \frac{B}{T} \tag{2}$$

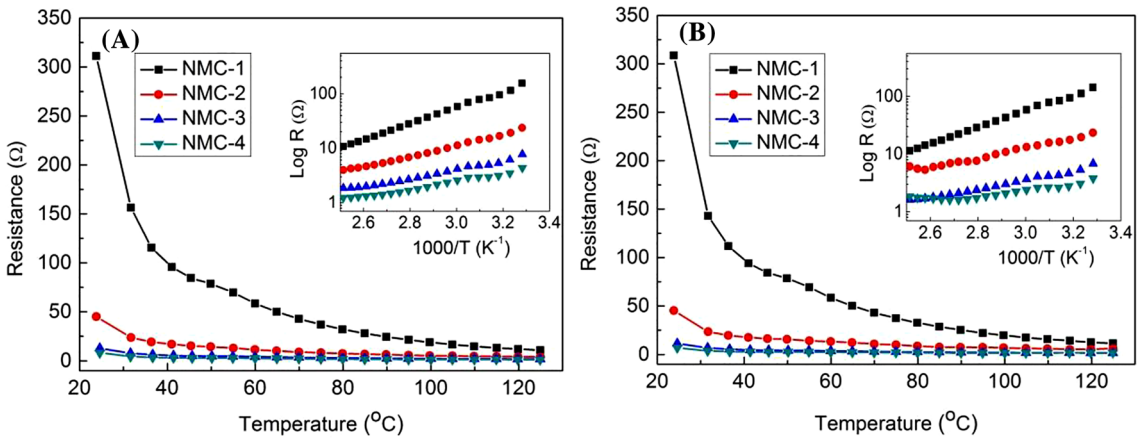

Fig. 1 Relationship between resistance (R) and testing temperature of $Ni_{0.7}Mn_{2.3-x}Cu_xO_2$ ($x=0.1$–0.4) ceramics: **a** pristine and **b** after aging. Inset is the change in logR as a function of the reciprocal of temperature (1/T)

where ρ_T is the resistivity at the temperature of T, T is the absolute temperature (K), A is a constant, k is the Boltzmann constant, E_a is the activation energy of conduction, and B is the thermistor constant. Accordingly, as shown in the insets in Fig. 1, the log$R$ varies almost linearly with the reciprocal of absolute temperature ($1/T$) between 25 and 130 °C.

On the other hand, the resistivity at room temperature of NMC-1, NMC-2, NMC-3, and NMC-4 samples were calculated as 780, 144, 21 and 15 Ω cm, respectively. This means that the resistivity decreases as Cu content increases. The electrical conductivity is associated with polaron hopping in nickel manganite ceramics. In other words, it depends mainly on ion concentration and hopping distance between trivalent and tetravalent Mn cations in the octahedral sites of crystal [7, 11]. Additionally, the valence state of cations in octahedral sites also affects the conductivity of material. After aged at 300 °C for 30 h in air atmosphere, it can be seen in Fig. 1b that all the samples have little tendency change in resistance. However, room temperature resistivity increased compared to pristine samples. The resistivity of NMC-1, NMC-2, NMC-3, and NMC-4 samples were calculated as 868, 166, 27, and 19 Ω cm, respectively, after aging at 300 °C for 30 h.

To further discuss the resistance–temperature characteristic of $Ni_{0.7}Mn_{2.2-x}Cu_xO_4$ NTC ceramic, thermistor constant (B-value) was calculated according to Eq. (3) [35, 36].

$$B = \frac{\ln \rho_{25} - \ln \rho_{85}}{\frac{1}{T_{25}} - \frac{1}{T_{85}}} \tag{3}$$

where ρ_{25} and ρ_{85} are the resistivities of NTC ceramics at 25 °C and 85 °C, respectively. The B-values of NMC-1, NMC-2, NMC-3, and NMC-4 samples were 4219, 3356, 2646, and 2469 K, respectively. The B-value also decreases as Cu content increases from 0.1 to 0.4. Therefore, B-value can be tailored by Cu content in $Ni_{0.7}Mn_{2.3-x}Cu_xO_4$ system, enabling to meet the different requirements for NTC ceramics.

The resistivity and B-value drifts of $Ni_{0.7}Mn_{2.3-x}Cu_xO_4$ samples after aging at 300 °C for 30 h are depicted in Fig. 2. Here, the drift is defined as Eqs. 4 and 5.

$$R_{drift} = \frac{R_{aging} - R_{origin}}{R_{origin}} \times 100\% \tag{4}$$

$$B_{drift} = \frac{B_{aging} - B_{origin}}{B_{origin}} \times 100\% \tag{5}$$

As can be seen, the drifts in both resistivity and B-value increase with increasing Cu content. The resistivity drift for NMC-1 sample was 13%, while the NMC-4 sample was up to 33%. However, after aging at 300 °C for 30 h, the B-value drift was 1.4%, 4.4%, 5.3%, and 9.1% for NMC-1, NMC-2, NMC-3, and NMC-4 samples, respectively. The B-value displayed higher stability than the resistivity. In general, B-value is associated with activation energy E_a, as expressed in Eq. (6).

$$B = \frac{E_a}{k} = \frac{1}{k}(U_s + \frac{1}{2}E_s) \tag{6}$$

Here, E_s and U_s are the formation energy and migration energy, respectively, and they are relatively constant for specific materials. Therefore, with less Cu content, the drift of B-value is extremely low for NMC-1 sample. The more content of Cu would lead to the increase of transition probability of localized carriers, reducing the activation energy E_a. As a result, the drift of B-value increases as Cu content increases.

The crystalline phases of prepared $Ni_{0.7}Mn_{2.3-x}Cu_xO_4$ ($x = 0.1$, 0.2, 0.3, and 0.4) ceramics were analyzed by X-ray diffraction (XRD, D8 Advance, Bruker, Germany) over the 2θ range from 10° to 80° at room temperature. As shown in Fig. 3, cubic spinel phases are successfully obtained for all the samples with different Cu contents, and no impurity phase is found, suggesting that Cu cations possible

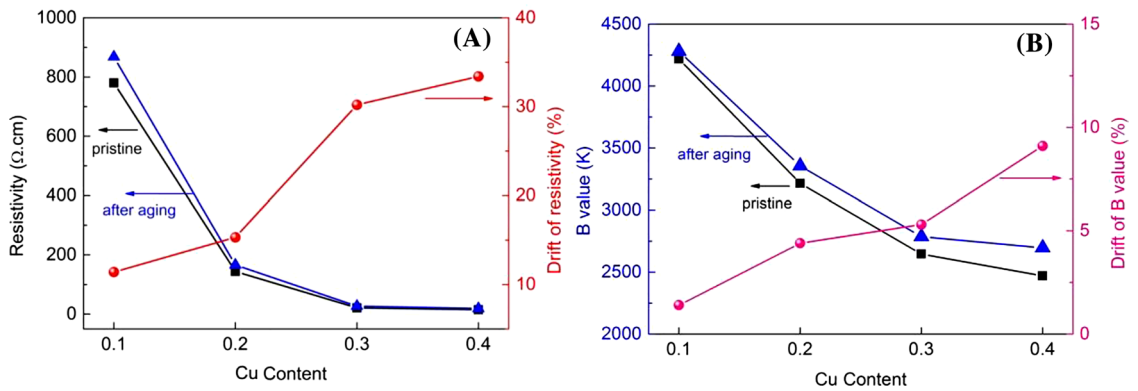

Fig. 2 Resistivity drift (**a**) and B-value drift (**b**) as a function of Cu content for $Ni_{0.7}Mn_{2.3-x}Cu_xO_4$ ($x = 0.1$, 0.2, 0.3, and 0.4) samples

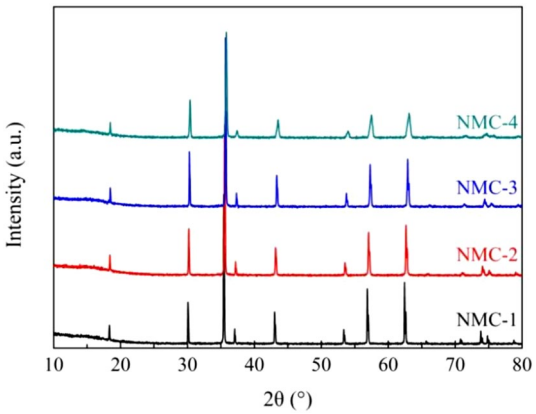

Fig. 3 XRD patterns of $Ni_{0.7}Mn_{2.3-x}Cu_xO_4$ ($x=0.1$, 0.2, 0.3, and 0.4) ceramics

incorporate into the lattice. Figure 4 shows the surface images of samples observed by field emission scanning electron microscopy (FESEM, JSM-7500F, JEOL, Japan). It can be seen that all the prepared samples are dense and less porosity, with grain sizes in micron scale. As Cu content increases, the grain size of sample increases from 1–2 μm to 3–4 μm, and has a narrower distribution. It is known that CuO has been often used as additive to facilitate sintering densification and grain growth. As a whole, greater grain size implies less proportion of grain boundary, thus resulting in less energy barrier to electrical conduction. Similar results were obtained in the Reference [37] as well, where $NiMn_2O_4$ sample with more uniform microstructure exhibited lower resistivity. In this sense, the resistivity decreases as Cu content increases. Especially, one can see that the microstructures of samples do not show obvious change subjecting to long-time aging. Hence, both the grain size and densification have little influence on the drift in resistivity and *B*-value.

The constituent chemical states of prepared ceramics were investigated using X-ray photoelectron spectroscopy (XPS, Thermo, ESCALAB 250XI, USA). The spectra of Mn $2p_{3/2}$ before and after aging are shown in Fig. 5. Obviously, Mn $2p_{3/2}$ spectra could be deconvoluted into two peaks at binding energies of 641.3 eV and 642.7 eV which assign to Mn^{3+} and Mn^{4+}, respectively. The conductivity of nickel manganite samples originates mainly from polaron hopping between Mn^{3+} and Mn^{4+}, so the resistivity is closely related to the concentration of trivalent and tetravalent Mn ions. Through calculating, the ratios of Mn^{3+} to Mn^{4+} for NMC-1 and NMC-3 samples are 1.11 and 0.60, respectively (Fig. 5a, b). Additionally, all the trivalent Mn ions did not participated in hopping process but assisted function was required by Mn^{4+} ions [38]. Hence, doping cations at octahedral sites may easily disrupt the equilibrium between Mn^{3+} and Mn^{4+} ions [21]. In this work, the resistivity of sample decreased as Cu content increased, implying that doping Cu ions were apt to occupy A sites of the tetrahedral, while Mn ions partially occupied both A and B sites. Jung et al. [39] reported that Ni^{2+} mainly occupied B site. Meanwhile, when Cu ions occupied at A sites, a part of Mn ions at A sites would migrate to B sites for maintaining electric neutrality, which leaded to an increase in Mn^{4+} concentration, contributing on conductivity.

XPS spectra of Mn $2p_{3/2}$ for the samples after aging are shown in Fig. 5c, d. The ratios of Mn^{3+} to Mn^{4+} for NMC-1 and NMC-3 samples reach to 1.28 and 0.84, respectively, after aging. This illustrates that Mn^{4+} ions content becomes less. The increments in the ratios for NMC-1 and NMC-3 samples are 0.17 and 0.24, respectively. As aforementioned, Mn^{4+} content is responsible for electrical conduction, so it is reasonable that the resistivity change of NMC-3 sample is higher than that of NMC-1 sample. The results are well consistent with the resistivity-temperature relationship in Fig. 2.

Furthermore, XPS was carried out for NMC-4 samples before and after aging, to gain a better understand on the chemical states in $Ni_{0.7}Mn_{2.3-x}Cu_xO_4$ system, as shown in Fig. 6. One peak is only found which attributes to Cu^+ for the sample before aging. After aging, Cu $2p_{3/2}$ could be deconvoluted into two peaks at binding energies of 932.3 eV and 934.1 eV, which assign to Cu^+ and Cu^{2+}, respectively. This indicates that the chemical valence of Cu ion increases after aging. While the valence of Cu ion increases from + 1 to + 2, the content of Mn^{4+} ions reduces for charge balance, in agreement with the change in chemical states of Mn ions after aging. Apparently, the increase in conductivity would result in the greater drift in both resistivity and B-value.

4 Conclusions

$Ni_{0.7}Mn_{2.3-x}Cu_xO_2$ ($x=0.1$, 0.2, 0.3, and 0.4) NTC ceramics were prepared by solid-state method. And the as-prepared samples were heat-treated at 300 °C for 30 h in air atmosphere to investigate their aging characteristics. Results showed that the resistivities of NMC-1, NMC-2, NMC-3, and NMC-4 samples were 780, 144, 21, and 15 Ω•cm, respectively. However, the drift in both the resistivity and B-value increased as Cu content increased. SEM observation demonstrated that the grain size and densification had little influence on the performance degradation. Through XPS analysis, it was convinced that after aging, Cu^+ ions in system were oxidized to Cu^{2+} ions, which gave rise to the decrease of Mn^{4+} content, contributing to the greater drift in resistivity and B-value. The findings indicate that stabilizing the chemical state of Mn^{4+} could efficiently suppress the degradation of electrical properties for nickel manganite NTC ceramics.

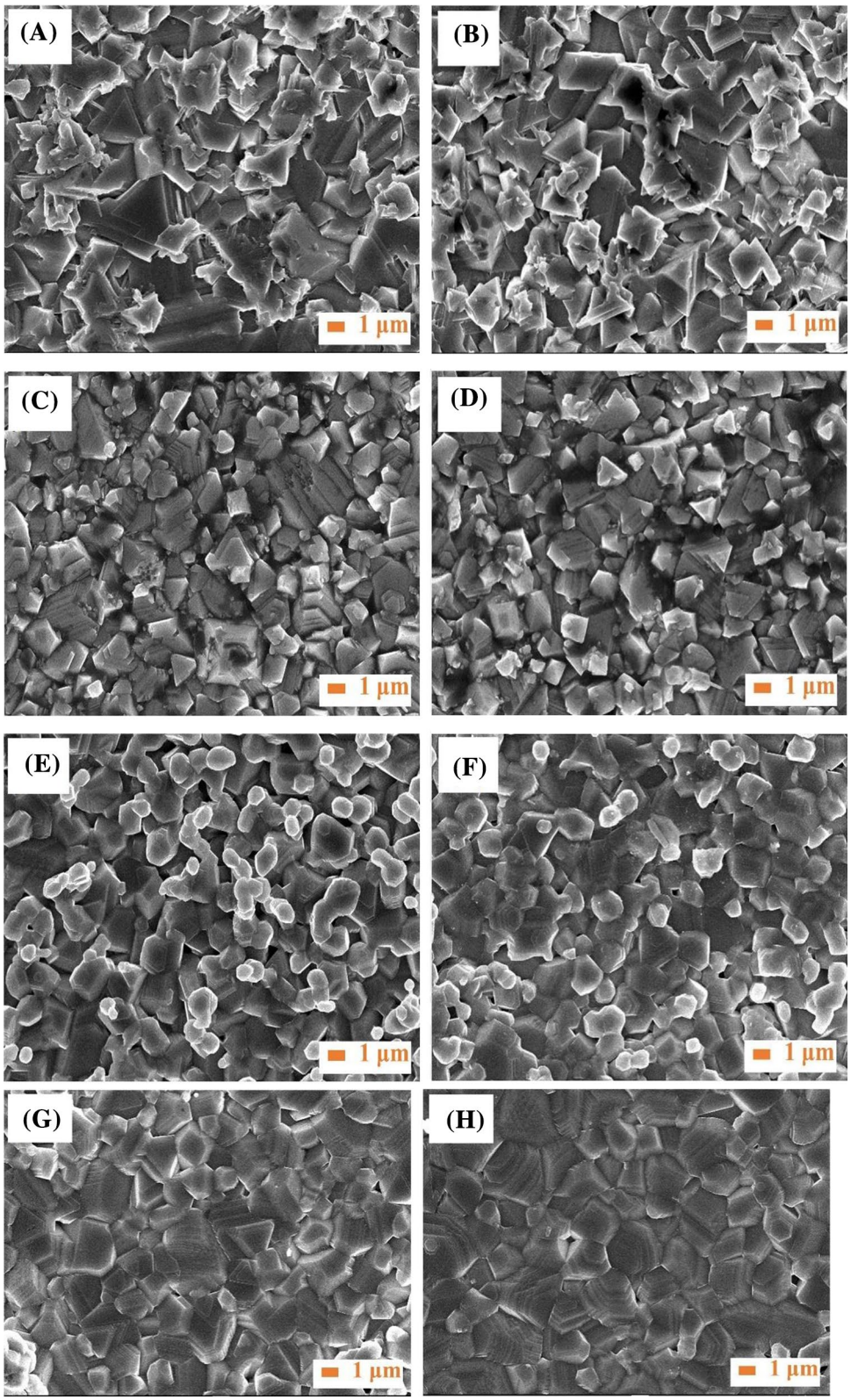

Fig. 4 SEM images of as-prepared $Ni_{0.7}Mn_{2.3-x}Cu_xO_4$ ($x=0.1$, 0.2, 0.3, and 0.4) ceramics. **a**, **c**, **e** and **g** are pristine samples and **b**, **d**, **f** and **h** are aged samples corresponding to $x=0.1$, 0.2, 0.3, and 0.4, respectively

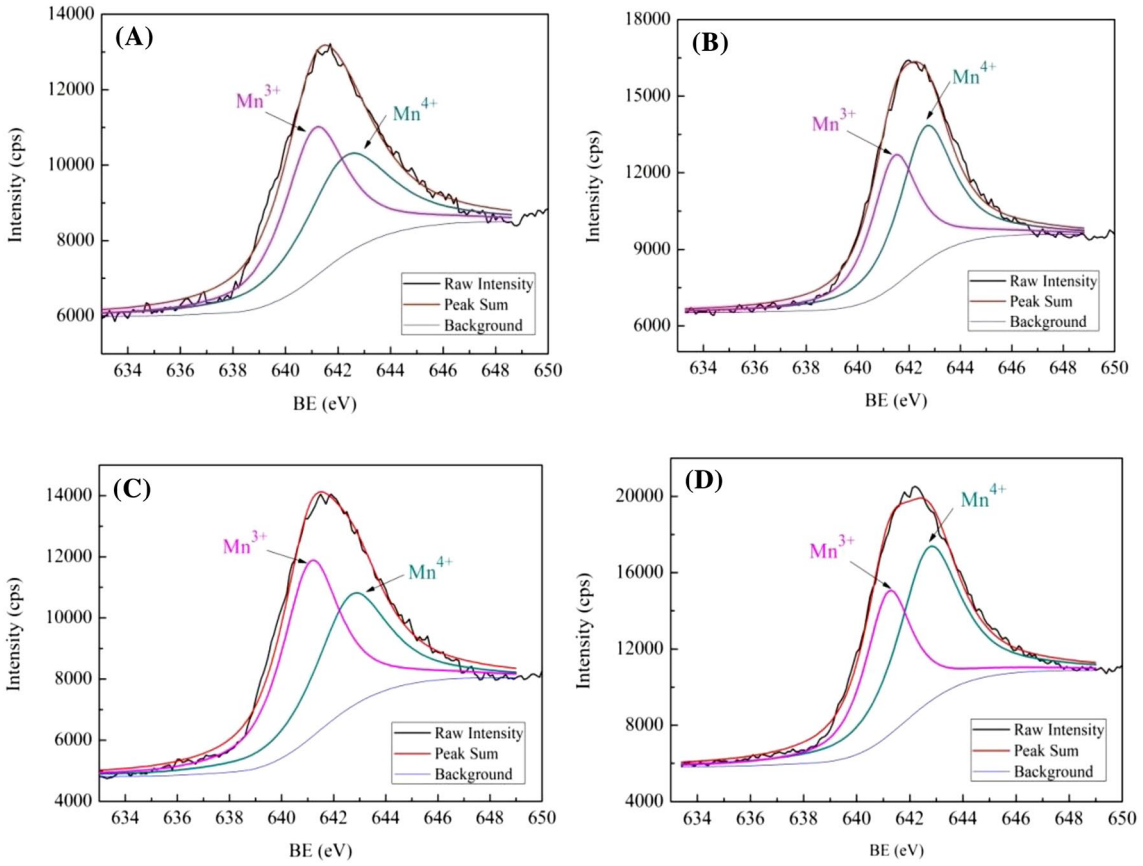

Fig. 5 XPS spectra of Mn $2p_{3/2}$ of NMC-1 (**a**) and NMC-3 (**b**) samples before aging and NMC-1 (**c**) and NMC-3 (**d**) samples after aging

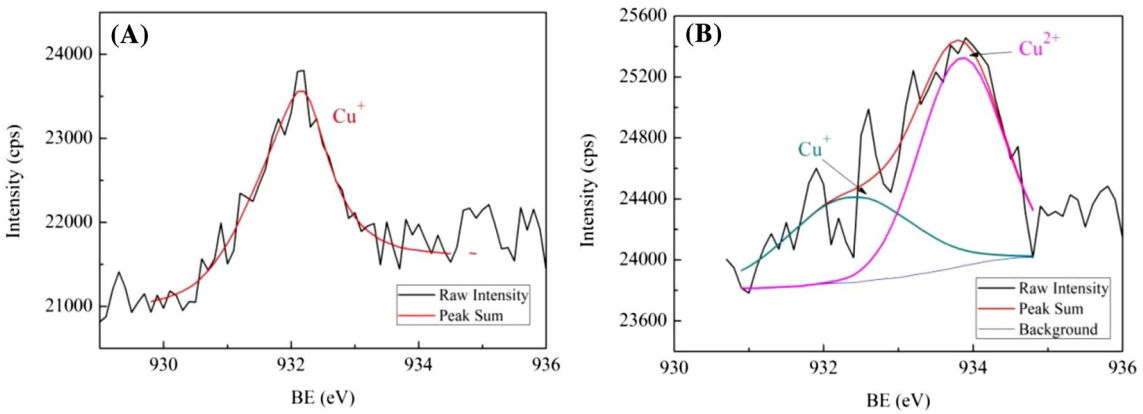

Fig. 6 XPS spectra of Cu $2p_{3/2}$ for NMC-4 samples before (**a**) and after (**b**) aging

Acknowledgements Authors would like to acknowledge the financial support of the National Natural Science Foundation of China (Grant No.61974114)

References

1. J.A. Becker, C.B. Green, G.L. Pearson, Properties and uses of thermistors-thermally sensitive resistors. Electr. Eng. **65**, 711–725 (1946)
2. F. Guan, X. Lin, H. Dai, J. Wang, X. Cheng, S. Huang, $LaMn_{(1-x)}TixO_{(3)}$-$NiMn_2O_4$($0 \le x \le 0.7$): a composite NTC ceramic

with controllable electrical property and high stability. J. Eur. Ceram. Soc. **39**, 2692–2696 (2019)
3. K. Park, I.H. Han, Effect of partial substitution of Mg for Co in $Mn_{1.4}Ni_{1.2}Co_{0.4}O_4$ NTC thermistors on electrical stability. J. Electroceram. **17**, 1079–1082 (2006)
4. P. Li, H. Zhang, C. Gao, G. Jiang, Z. Li, Electrical property of Al/La/Cu modified ZnO-based negative temperature coefficient (NTC) ceramics with high ageing stability. J. Mater. Sci. Mater. Electron. **30**, 19598–19608 (2019)
5. A. Petar, M. Pedja, Temperature compensation of NTC thermistors based anemometer. Sens. Actuators, A **285**, 210–215 (2019)
6. S. Liang, X. Zhang, Y. Bai, Z. Han, J. Yang, Study on the preparation and electrical properties of NTC thick film thermistor deposited by supersonic atmospheric plasma spraying. Appl. Surf. Sci. **257**, 9825–9829 (2011)
7. C. Ma, Y. Liu, Y. Lu, H. Gao, H. Qian, J. Ding, Effect of Zn substitution on the phase, microstructure and electrical properties of $Ni_{0.6}Cu_{0.5}Zn_xMn_{1.9-x}O_4 (0 \le x \le 1)$ NTC ceramics. Mater. Sci. Eng. B **188**, 66–71 (2014)
8. L. Chen, J. Wang, C. Huang, Q. Zhang, S. Chang, A. Chang, J. Yao, High performance of $Ni_{0.9}Mn_{1.8}Mg_{0.3}O_4$ spinel nanoceramic microbeads via inkjet printing and two step sintering. RSC Adv. **6**, 35118–35123 (2016)
9. K. Park, I.H. Han, Effect of Cr_2O_3 addition on the microstructure and electrical properties of Mn-Ni-Co oxides NTC thermistors. J. Electroceram. **17**, 1069–1073 (2006)
10. H. Gao, C. Ma, B. Sun, Preparation and characterization of $NiMn_2O_4$ negative temperature coefficient ceramics by solid-state coordination reaction. J. Mater. Sci. Mater. Electron. **25**, 3990–3995 (2014)
11. R.N. Jadhav, V. Puri, Influence of copper substitution on structural, electrical and dielectric properties of $Ni_{(1-x)}Cu_xMn_2O_4$ ($0 \le x \le 1$) ceramics. J. Alloy. Compd. **507**, 151–156 (2010)
12. C. Ma, Y. Liu, Y. Lu, Preparation routes and electrical properties for $Ni_{0.6}Mn_{2.4}O_4$ NTC ceramics. J. Mater. Sci. Mater. Electron. **26**, 7238–7243 (2015)
13. M. Ji, W. Ren, L. Li, Y. Wang, X. Zhang, Q. Zhou, J. Hu, C. Jiang, Formation of highly textured $Zn_{0.2}Ni_{0.8}Mn_2O_4$ thin films by RF magnetron sputtering. ECS J. Solid State Sci. Technol. **7**, 114–116 (2018)
14. K. Park, J.K. Lee, S.J. Kim, W.S. Seo, W.S. Cho, C.W. Lee, S. Nahm, The effect of Zn on the microstructure and electrical properties of $Mn_{1.17-x}Ni_{0.93}Co_{0.9}Zn_xO_4$ ($0 \le x \le 0.075$) NTC thermistors. J. Alloys Compd. **467**, 310–316 (2009)
15. C. Zhao, Y. Zhao, The investigation of Zn content on the structure and electrical properties of $Zn_xCu_{0.2}Ni_{0.66}Mn_{2.14-x}O_4$ negative temperature coefficient ceramics. J. Mater. Sci. Mater. Electron. **23**, 1788–1792 (2012)
16. A. NgueteuKamlo, J. Bernard, C. Lelievre, D. Houive, Synthesis and NTC properties of $YCr_{1-x}Mn_xO_3$ ceramics sintered under nitrogen atmosphere. J. Eur. Ceram. Soc. **31**, 1457–1463 (2011)
17. S. Liang, X. Zhang, H.B. Li, M. Luo, J. Li, L.J. He, J.F. Yang, Fabrication and characterization of Ni-Mn-Si-Al-O NTC thermistor and its application as temperature wire sensor. Funct. Mater. Lett. **6**, 1350039 (2013)
18. X. Sun, S. Leng, H. Zhang, Z. He, Z. Li, Electrical properties and temperature sensitivity of Li/Mg modified $Ni_{0.7}Zn_{0.3}O$ based ceramics. J. Alloys Compd. **763**, 975–982 (2018)
19. C. Ma, Y. Liu, Y. Lu, H. Qian, Preparation and electrical properties of $Ni_{0.6}Mn_{2.4-x}Ti_xO_4$ NTC ceramics. J. Alloys Compd. **650**, 931–935 (2015)
20. R.N. Jadhav, S.N. Mathad, V. Puri, Studies on the properties of $Ni_{0.6}Cu_{0.4}Mn_2O_4$ NTC ceramic due to Fe doping. Ceram. Int. **38**, 5181–5188 (2012)
21. M.A. Rafiq, M.T. Khan, Q.K. Muhammad, M. Waqar, F. Ahmed, Impedance analysis and conduction mechanism of Ba doped $Mn_{1.75}Ni_{0.7}Co_{0.5-x}Cu_{0.05}O_4$ NTC thermistors. Appl. Phys. A-Mater. Sci. Process. **123**, 589 (2017)
22. P.B. Yuksel, H. Gokhan, Preparation and characterization of Ni-Co-Zn-Mn-O negative temperature coefficient thermistors with B_2O_3 addition. J. Mater. Sci.: Mater. Electron. **30**, 17432–17439 (2019)
23. J. Chen, J. Wang, J. Yao, A. Chang, B. Wang, Pd/Ag thin film deposited on negative temperature coefficient (NTC) ceramics by direct current magnetron sputtering. Vacuum **167**, 227–233 (2019)
24. T. Liu, H. Zhang, P. Ma, A. Chang, H. Jiang, Core-shell NTC materials with low thermal constant and high resistivity for wide-temperature thermistor ceramics. J. Am. Ceram. Soc. **102**, 4393–4398 (2019)
25. R. Metz, Electrical properties of N.T.C. thermistors made of manganite ceramics of general spinel structure: $Mn_{3-x-x'}M_xN_{x'}O_4$ ($0<x+x'<1$; M and N being Ni, Co or Cu). Aging phenomenon study. J. Mater. Sci. **35**, 4705–4711 (2000)
26. S. Michaela, M. Christian, S. Sophie, P. Veronique, K. Jaroslaw, M. Ralf, Characterization of nickel manganite NTC thermistor films prepared by aerosol deposition at room temperature. J. Eur. Ceram. Soc. **38**, 613–619 (2018)
27. S. Michaela, M. Christian, S. Sophie, P. Veronique, K. Jaroslaw, M. Ralf, Novel method for NTC thermistor production by aerosol co-deposition and combined sintering. Sensors **19**, 1632 (2019)
28. S. Michaela, M. Christian, S. Sophie, P. Veronique, K. Jaroslaw, M. Ralf, Thermal treatment of aerosol deposited $NiMn_2O_4$ NTC thermistors for improved aging stability. Sensors **18**, 3982 (2018)
29. A.V. Salker, S.M. Gurav, Electronic and catalytic studies on $Co_{1-x}Cu_xMn_2O_4$ for CO oxidation. J. Mater. Sci. **35**, 4713–4719 (2000)
30. G. Na, Y.D. Li, Effects of Cd and Cd-Cu doping on the microstructure and electrical properties of NiMnCoO NTC ceramics. Adv. Mater. Res. **236–238**, 1632–1635 (2011)
31. R. Jadhav, D. Kulkarni, V. Puri, Structural and electrical properties of fritless $Ni_{(1-x)}Cu_xMn_2O_4$ ($0 \le x \le 1$) thick film NTC ceramic. J. Mater. Sci. Mater. Electron. **21**, 503–508 (2010)
32. C. Zhao, B. Wang, P. Yang, L. Winnubst, C. Chen, Effects of Cu and Zn co-doping on the electrical properties of $Ni_{0.5}Mn_{2.5}O_4$ NTC ceramics. J. Eur. Ceram. Soc. **28**, 35–40 (2008)
33. G. Wang, H. Zhang, X. Sun, Y. Liu, Z. Li, Characterization of a new system of NTC temperature-sensitive ceramics based on Al/F modified NiO simple oxides. J. Mater. Sci. Mater. Electron. **28**, 363–370 (2017)
34. K. Park, D.Y. Bang, Electrical properties of Ni-Mn-Co-(Fe) oxide thick-film NTC thermistors prepared by screen printing. J. Mater. Sci. Mater. Electron. **14**, 81–87 (2003)
35. F. Cheng, J. Wang, H. Zhang, A. Chang, W. Kong, B. Zhang, L. Chen, Phase transition and electrical properties of $Ni_{1-x}ZnxMn_2O_4$ ($0 \le x \le 1.0$) NTC ceramics. J. Mater. Sci. Mater. Electron. **26**, 1374–1380 (2015)
36. J. Wang, J. Zhang, Structural and electrical properties of $NiMg_xMn_{2-x}O_4$ NTC thermistors prepared by using sol-gel derived powders. Mater. Sci. Eng. B **176**, 616–619 (2011)
37. C. Ma, H. Gao, Preparation and characterization of single-phase $NiMn_2O_4$ NTC ceramics by two-step sintering method. J. Mater. Sci. Mater. Electron. **28**, 6699–6703 (2017)
38. H.R. Jung, S.G. Lee, K.M. Kim, M.S. Kwon, Y.G. Kim, Preparation and electrical properties of nickel manganite $Ni_{0.79}Mn_{2.21}O_4$ ceramics for NTC thermistors. J. Ceram. Process. Res. **18**, 357–360 (2017)
39. H.R. Jung, S.G. Lee, D.J. Lee, Y.O. Jo, Structural and electrical properties of nickel manganite ceramics for NTC thermistor material. Sci. Adv. Mater. **9**, 1346–1349 (2017)